Metall. Res. Technol. **111**, 305–310 (2014)
© EDP Sciences, 2014
DOI: 10.1051/metal/2014041
www.metallurgical-research.org

&Metallurgical Research Technology

Sintering of ferritic and austenitic nanopowders using Spark Plasma Sintering

B. Mouawad[1], D. Fabregue[1], M. Perez[1], M. Blat[2], F. Delabrouille[2], C. Domain[2] and C. Pokor[2]

[1] *Université de Lyon-INSA de Lyon-MATEIS UMR CNRS 5510, 69621 Villeurbanne, France*
e-mail: bassem.mouawad@insa-lyon.fr
[2] *EDF R&D Dpt. MMC, Les Renardières, 77818 Moret sur Loing, France*

Key words:
316L nanopowder steels; non-ODS steels; Spark Plasma Sintering; nano-sized microstrucure

Received 24 December 2013
Accepted 8 October 2014

Abstract – This study aims at presenting a way to obtain nanostructured materials. Austenitic stainless steel (316L) nanopowders and ferritic/martensitic alloy steels (Fe14Cr) are sintered with the Spark Plasma Sintering (SPS) technique. This technique leads to a fully dense/nano-sized microstructure material after a short treatment. The optimal sintering temperature was found to be 850°C for both materials. The relationship between the Vickers Hardness and scale of the microstructure is in good agreement with the Hall-Petch Law.

In a nuclear reactor, some components are exposed to high doses of irradiation (>100 dpa) in their operating life, causing an alteration of the original properties, and leading to a drastic drop in their mechanical properties. Nanomaterials may be a solution to the problem since the materials seem to be able to resist radiation damage [1].

The aim of this study is to produce two kinds of nanostructured materials: austenitic and ferritic stainless steels. Austenitic stainless steels (316L) are usually used to maintain the fuel assemblies in the internal structures of Pressurized Water Reactors (PWRs). The radiation resistance of these austenitic nanostructured materials will be studied within the horizon of the Long-Term Operation (LTO) strategy of PWRs. Concerning the ferritic/martensitic alloy steels, Oxide Dispersion Strengthened (ODS) steels are the main candidate materials for fuel cladding for the Sodium Fast Reactors (SFRs) [2]. Sintering studies of ODS steels have been reported by many authors [3–5]. Here, non-ODS Fe-14%Cr steels were chosen as the second alloy, to study the effect of grain boundaries without the nano-reinforcements.

Sintering of these two materials has already been reported in the literature. Sintering of 316L stainless steel to near fully dense material has been reported using a conventional sintering technique. A relative density of 84% and 96.14% can be achieved for a sintering temperature of 1200 and 1250°C, respectively, for more than an hour [6,7]. Akhtar et al. enhanced the density of sintered 316L at high temperature by using additional elements [8]. Moreover, the sintering of 316L nanopowders has also been reported using the Hot Isostatic Pressing (HIP) process [9]. Concerning the non-ODS ferritic steels, Auger et al. studied the sintering of ODS and non-ODS steels using HIP and SPS, at a temperature of 1100°C [5,10].

In this paper, we present a sintering study for austenitic and ferritic nanostructured materials using the SPS process with different sintering parameters, especially at low temperature and in a short time, in order to obtain fully dense materials with a fine microstructure.

1 Materials and methods

1.1 Steel powders

As we mentioned before, two types of steel powders were used in this study. The first is an austenitic stainless steel nanopowder (316L from SkySpring Nanomaterials Inc.,

https://doi.org/10.1051/metal/2014041 Published online by Cambridge University Press
Article published by EDP Sciences

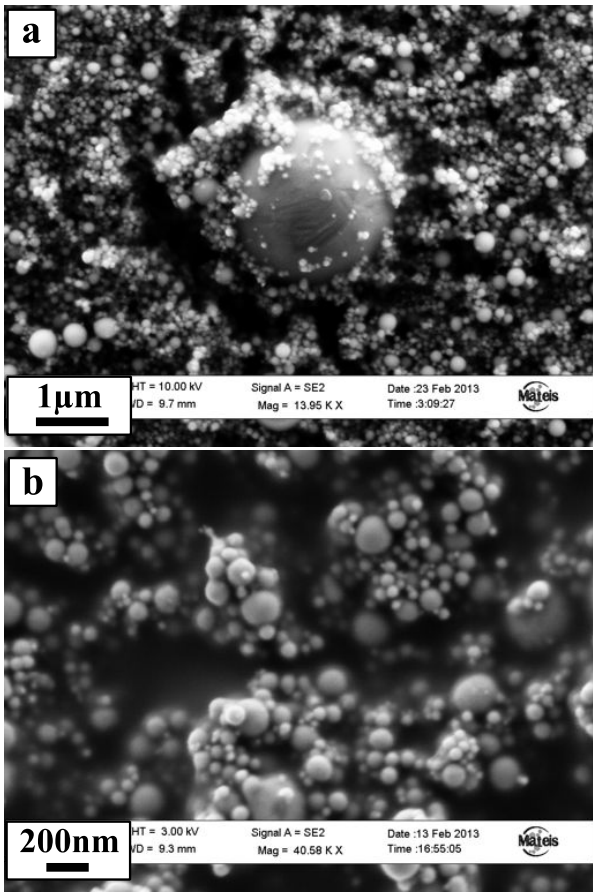


Fig. 1. SEM image of 316L nanopowders showing initial powder structure on two different scales.

USA) obtained by electrical wire explosion (spherical shape). Figure 1 illustrates the structure of the 316L initial nanopowders.

The second material is a ferritic stainless steel powder produced by Mechanical Alloying (MA) of a gas-atomized prealloyed steel Fe-14Cr-1W, by Aubert and Duval. Then, the ferritic powder was milled at CEA Saclay using a high-energy attrition mill at 400 rpm for 10 hours, under an argon atmosphere. Steel balls (440C) with 8 mm diameter were used in this work and the ball-to-powder mass ratio was 15. This process gives highly deformed granules with asymmetric shapes. Figure 2 a shows a SEM image of the milled powders with a particle size mostly equal to 200 μm. It should be noted that the original powders contain a high density of dislocations due to MA.

The chemical composition of both stainless steels given by the suppliers is reported in Table 1.

1.2 Sintering process

The powders were sintered using a FCT Systeme GmbH SPS model HP D 25, without any additives. For both steels, powders were consolidated using a cylindrical graphite die, with an inner diameter of 10 mm, under vacuum (10^{-2} mbar). The goal is to form cylindrical pellets of 2.6 mm height. The sintering process was performed using a holding pressure of 90 MPa, a dwell time of 5 min and a heating rate of 700°C/min, and a holding temperature was chosen equal to 850, 950 or 1050°C for both steel. In addition, a holding temperature of 750°C was also tested for the 316L steel. The temperature was controlled by a horizontal pyrometer targeting inside a hole in the graphite die, close to the powder.

After the 5 min holding time at a chosen sintering temperature, the whole system (graphite die and cylindrical pellets) was cooled down to room temperature by direct contact with water-cooled punches.

1.3 Density

At the end of the sintering process, samples were slightly polished in order to remove any carbon residual the SPS carbon tooling may have produced. Then, precise density measurements were made using the Archimedes principle according to ASTM Standard B328-94. The relative density was calculated based on the theoretical density of 316L (7990 kg/m^3) and Fe14Cr (7795 kg/m^3).

1.4 Microhardness

At the end of the sintering process, samples were cross-sectioned, mounted in a hot mounting conductive resin and then prepared metallographically (mechanical grinding and polishing down to 0.06 μm silica slurry). Diamond pyramid Vickers microhardness measurements were performed with a Buehler 5100 semi-automated testing instrument. The microhardness values for the consolidated samples with 0.06 μm diamond surface finish, at a 1000-g load, were based on the average of a minimum of ten indents.

https://doi.org/10.1051/metal/2014041 Published online by Cambridge University Press

Table 1. Chemical composition (weight %) of austenitic and ferritic stainless steel as given by the suppliers.

Elements	Fe	Cr	W	Ni	Mo	Mn	Si	P	S	Ti	C
316L	bal.	16–18	–	10–14	2–3	2	0.75	0.045	0.03	–	0.03
Fe14Cr1W	bal.	14	1	0.15	–	0.3	0.3	–		0.02	ppm

1.5 Powder and microstructure characterization

Both powders were observed using a scanning electron microscope (SEM) Zeiss Supra 55 VP with a field emission gun (FEG) with a tension of 3–10 kV. In order to characterize the microstructure of the as-milled ferritic stainless steel, a powder particle was milled by focused ion beam (FIB) and characterized using a SEM-FEG associated with an Electron Back-Scattered Diffraction (EBSD) Oxford system for orientation and grain size measurement (12 kV with a step size of 25–30 nm). All EBSD maps were performed at the center of the cross-sectional samples.

Grain size distributions were measured by EBSD and calculated with the post-processing software Channel 5. The size distribution was plotted in volume fractions. Therefore, the mean diameter D^V_{mean} was calculated as [11]:

$$D^V_{\text{mean}} = \frac{\sum_{i=1}^{m} (N_i D_i^3) D_i}{\sum_{i=1}^{m} N_i D_i^3} = \sum_{i=1}^{m} f_i^V D_i \quad (1)$$

where N_i, f_i^V and D_i are the number of grains, the volume fraction and the average diameter of each class i, respectively.

2 Results

2.1 As-received powders

The average particle size of 316L stainless steel nanopowders was equal to 60–80 nm. Thereby, large particles (>1 μm) were observed with nanopowders (cf. Fig. 1a).

For the Fe14Cr stainless steel, different EBSD maps were performed on the cross-sectional FIB milled particle (cf. Fig. 2b) using a low tension of 1.5 kV and a step of 15 nm. The histogram shown in Figure 2c was the sum of all EBSD data maps. The grain size distribution is relatively wide, with grain diameters from 20 to 980 nm. It

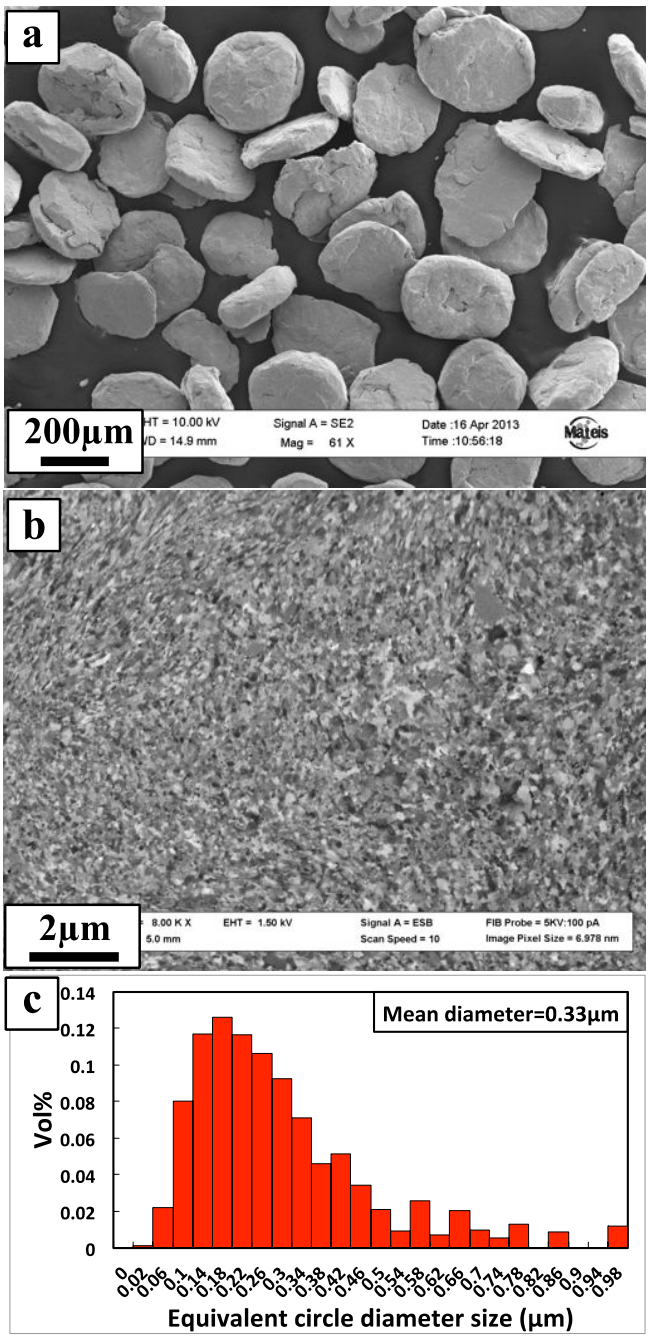


Fig. 2. SEM image of (a) as-milled Fe14Cr powders showing an asymmetric particle's shape and (b) the nano-crystallites inside a particle powder observed from focused ion beam (FIB) cross-section. The histogram shown in (c) presents the crystallite size distribution.

https://doi.org/10.1051/metal/2014041 Published online by Cambridge University Press

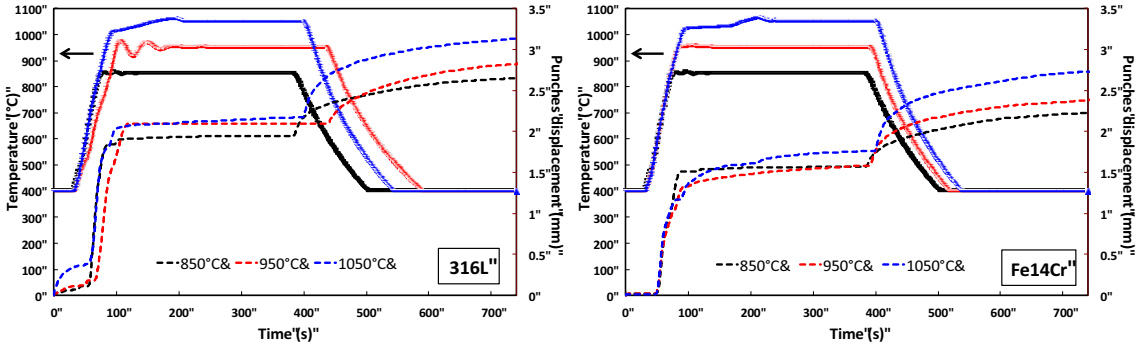


Fig. 3. Evolution of the relative punches' displacement at different sintering temperatures as a function of the SPS cycle time for both steels.

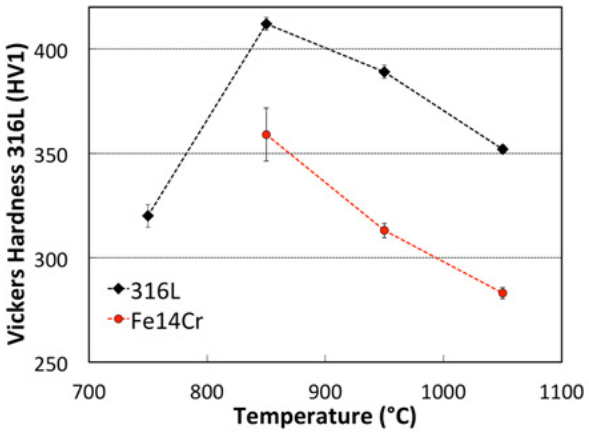


Fig. 4. Evolution of Vickers Hardness as a function of the sintering temperature for both steels. Error bars indicate the 95% confidence intervals.

should be noted that the 200 μm-Fe14Cr particles are polycrystalline with grains around 330 nm. The mean diameter was calculated according to Equation (1). It should be noticed that black pixels were found in all EBSD maps. This corresponds to the highly deformed grains due to the mechanical alloying that could not be indexed.

2.2 Density

Table 2 shows the relative density of austenitic and ferritic steel as a function of the sintering temperature. For sintering at 750°C, the relative density of 316L was low (85%). However, as the sintering temperature increases, near fully dense samples can be obtained at 850°C. The relative density of 316L and Fe14Cr were therefore

Table 2. Relative density of austenitic and ferritic stainless steel as function of sintering temperature.

Relative density (%)		
Sintering temperature (°C)	316L	Fe14Cr1W
750	85.4	93.6
850	93	988
950	93.9	99
1050	93.3	98.9

93% and 98.8% respectively. With increasing temperature, a small amount of carbon was transferred to the materials due to the SPS graphite materials (≈100 μm according to [12]). It should be noted that this amount was removed while polishing samples before the measurement of the density. Figure 3 shows the evolution of the relative punches' displacement as a function of the SPS cycle time for both powders for different sintering temperatures.

2.3 Vickers hardness

Figure 4 shows the Vickers Hardness for both steels as a function of the temperature. For the 316L steels, the lowest hardness value for 316L at 750°C is certainly related to the non-fully dense structure of the sample. Otherwise, at 850°C, the hardness was equal to 412 Hv1, twice the hardness of regular bulk 316L, where the hardness was equal to ≈160Hv10 and ≈190Hv10 when the average grain size was equal to 29 μm and 18.3 μm respectively [13], which constitutes the maximal value of this study. At 950°C, the hardness was equal to 388 Hv1, which is

https://doi.org/10.1051/metal/2014041 Published online by Cambridge University Press

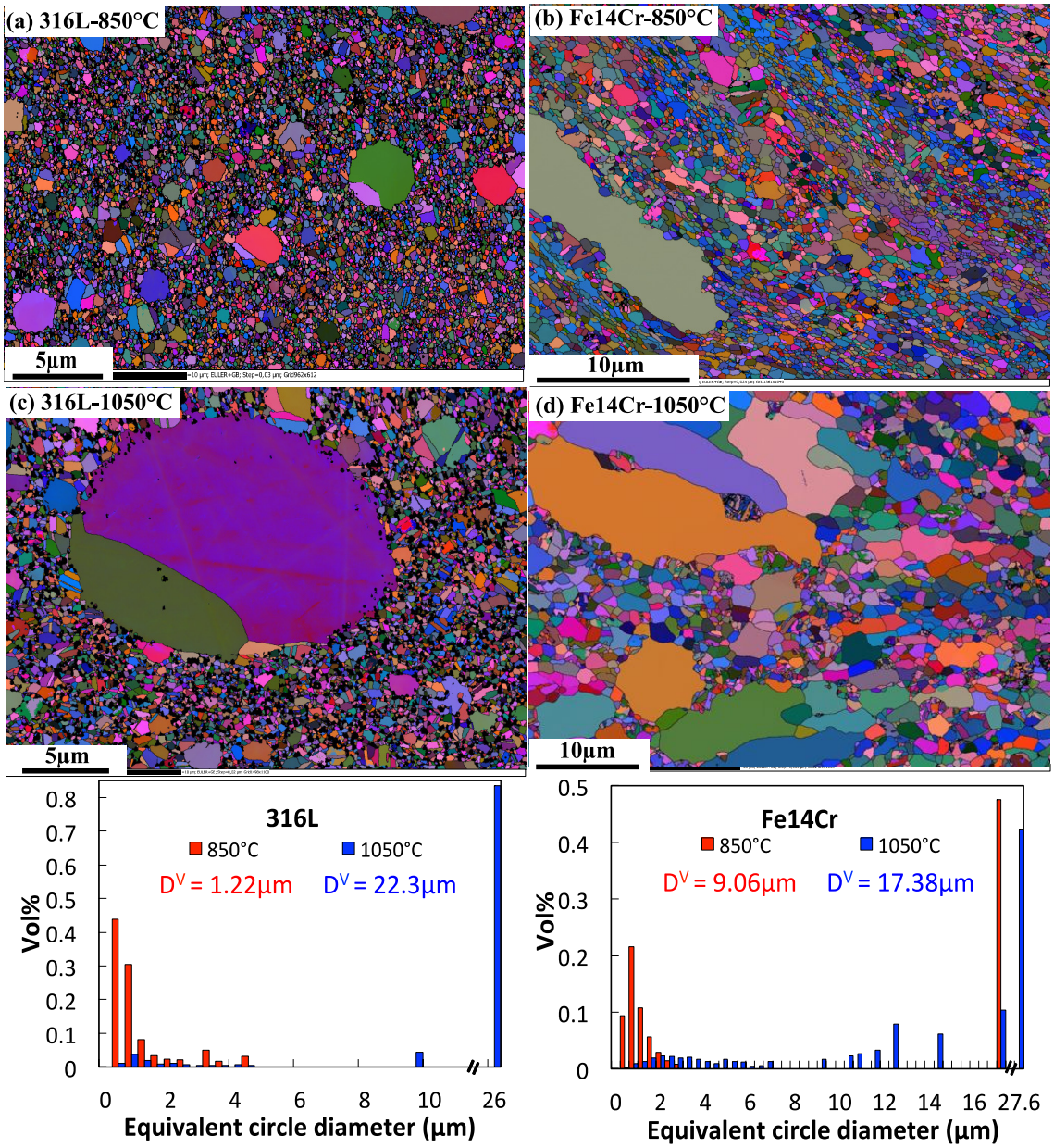


Fig. 5. Cross-sectional EBSD maps for sintered samples at two different temperatures (a–c) 316L and (b–d) Fe14Cr respectively. The grain size distribution is illustrated for both materials.

very similar to that obtained in [9] while sintering the 316L nanopowders using the HIP technique at the same temperature. For the Fe14Cr steels, the highest hardness value of 360 Hv1 was found at 850°C.

In both cases, the hardness decreases with increasing temperature. This result is completely coherent with the heat treatment of any material. Hence, the higher the holding temperature, the faster the grain growth phenomena occur. The evolution of the hardness appears to be related to the size of grains as shown in Figure 5.

2.4 Microstructure

Figure 5 shows EBSD maps of both steels sintered by SPS at 850°C for 5 min, for which the highest relative densities were obtained, and at 1050°C for 5 min showing the evolution of the microstructure at higher temperature. The relevant grain size distribution has

https://doi.org/10.1051/metal/2014041 Published online by Cambridge University Press

been inserted. In both cases, the microstructure exhibits a mix of nano-sized and coarse grains as we can see in Figures 5a and 5b, which certainly improves the mechanical properties of the sintered sample. The mean diameter was calculated according to Equation (1). For the 316L microstructure, the mean diameter was found to be equal to 1.22 μm. The higher diameter size is mainly due to the grain growth of the large grains shown in Figure 1 a. For the Fe14Cr microstructure, the mean diameter was equal to 9.06 μm. This value was extremely influenced by the large recrystallized grain present in the microstructure (17 μm). If, for example, the large grain was not taken into consideration, the mean diameter would be 600 nm.

3 Conclusion

Austenitic and ferritic powders were consolidated separately by SPS. The microstructure of both steels provides nano-sized and coarser grains. This microstructure leads to very good mechanical properties (better than bulk with micron grain size) and may be very attractive for resisting against radiation damage. Irradiation damage resistance will be studied in a forthcoming paper in order to see how well such nanostructured materials behave at different radiation doses.

Acknowledgements

This investigation was supported by EDF R&D (Project PERFORM-60: EDF R&D P10VB and EDF R&D P10VC). The authors are pleased to acknowledge important contributions used in the body of this work from G. Bonnefont and F. Mercier from MATEIS for SPS processing. Thanks are also due to the CLYM (Centre Lyonnais de Microscopie) and specially to T. Douillard for access to the FIB/SEM device used in this study.

References

[1] G. Ackland, *Sci. Mag.* **327** (2010) 1587

[2] P. Dubuisson, Y. DeCarlan, V. Garat, M. Blat, *J. Nucl. Mater.* **428** (2012) 6

[3] X. Boulnat, M. Perez, D. Fabrègue, T. Douillard, M.H. Mathon, Y. DeCarlan, *Metall. Mater. Trans. A* **45** (2014) 1485

[4] Q.X. Sun, T. Zhang, X.P. Wang, Q.F. Fang, T. Hao, C.S. Liu, *J. Nucl. Mater.* **424** (2012) 279

[5] M.A. Auger, V. de Castro, T. Leguey, A. Muñoz, R. Pareja, *J. Nucl. Mater.* **436** (2013) 68

[6] S. Pandya, K.S. Ramakrishna, A.R. Annamalai, A. Upadhyaya, *Mater. Sci. Eng. A* **556** (2012) 271

[7] C.H. Ji, N.H. Loh, K.A. Khor, S.B. Tor, *Mater. Sci. Eng. A* **311** (2001) 74

[8] F. Akhtar, L. Ali, F. Peizhong, J.A. Shah, *J. Alloys Compd.* **509** (2011) 8794

[9] H. Krztonìa, D. Kolesnikow, J. Paduch, R. Molend, J. Achiev, *Mater. Manuf. Eng.* **21** (2007) 73

[10] M.A. Auger, T. Leguey, A. MunÞoz, M.A. Monge, V. de Castro, P. Fernaìndez, G. Garceìs, R. Pareja, *J. Nucl. Mater.* **417** (2011) 213

[11] O.M. Sokovnin, N.V. Zagoskina, *Theor. Found. Chem. Eng.* **36** (2002) 601

[12] Landolt-Börnstein, *Groupe III Condens. Matter* **26** (1990)

[13] K.K. Singh, S. Sangal, G. Murty, *Mater. Sci. Technol.* **18** (2002) 165

https://doi.org/10.1051/metal/2014041 Published online by Cambridge University Press